Generation of n-qubit W states using spin torque

Amritesh Sharma [*] and Ashwin A. Tulapurkar [†]
Solid State Devices Group, Department of Electrical Engineering, Indian Institute of Technology, Bombay, India

(Received 20 February 2020; accepted 28 May 2020; published 22 June 2020)

The W state is a symmetrically entangled multipartite state where a single excitation is shared by all parties. It is an important resource for various quantum algorithms and communication systems, and hence, its preparation is of immense interest to the quantum information community. We examine here a deterministic scheme to prepare a W state of an n-qubit system with all-to-all pairwise exchange interaction between n qubits. This relies on sharing superposed excitations of a smaller number of q qubits among others. We present a bound on the maximal jumps from q to n and formalize a scheme to generate the W_n state in $O(\log n)$ stages. We demonstrate this scheme in the context of spin-torque-based quantum computing architecture that is characterized by repeated interactions between static and flying qubits.

DOI: 10.1103/PhysRevA.101.062330

I. INTRODUCTION

Quantum entanglement is purely a nonclassical phenomenon that enables many quantum information processing schemes and systems that exist today [1–3]. Generation of any arbitrary entangled state is an important problem, but certain entangled states are more useful. Two particularly inequivalent classes of tripartite entangled states, viz., Greenberger-Horne-Zeilinger and W, exist [4], and their generalizations to n qubits has been extensively investigated [5–7]. W states particularly have garnered interest in recent years because of their robustness against particle losses and local bit flips [8,9]. W_n states are defined as

$$W_n = \frac{1}{\sqrt{n}} \sum_{i=1}^{n} |0_1 0_2 \cdots 1_i 0_{i+1} \cdots 0_n\rangle. \tag{1}$$

Applications exploiting these properties are not limited to just secure quantum communication [10–12] and quantum teleportation [13,14]; ensemble-based quantum memories have also been proposed using these states [15]. They have also been used for addressing the leader-election problem [16], in addition to studying the fundamentals of quantum mechanics [5]. There exists proposals for and some experimental demonstrations of generating these states in several current competing noisy intermediate-scale [17] technologies like superconducting [8,18–21], photonic [22–28], and trapped ions [29,30] and so on. Implementations based on a universal-gate set of two-qubit and single-qubit operations can become complex as the system scales up [31,32]. Faster and simpler methods would involve a smaller number of architecture-oriented gates and multiqubit entanglement processes, as shown in [21]. Strategies exploiting lower-order W states to create higher-order W states can also be useful [26,28,33–35]. In addition, one circuit decomposition of an algorithm may not perform equally well for all implementations. So architecture-aware algorithms and hence circuit-decomposition strategies are warranted [36].

The realization of qubits using localized spins is a promising technology [3,37]. Manipulation and control of spins are therefore very important. "Classical" spin torque has played a key role in manipulating the magnetization of nanomagnets [38,39]. When spin-polarized current is injected into a ferromagnet (FM), the spin current polarized transverse to the magnetization direction of the FM is absorbed by it, leading to a spin torque. This is based on the exchange interaction between the conduction electrons and localized spins. Various mechanisms of producing spin-polarized current such as spin pumping [40], the spin Hall effect [41,42], spin-dependent thermoelectric effects [43], the spin Nernst effect [44,45], etc., have been studied in detail. It has been shown that spin torque in quantum systems can be used for single- and two-qubit manipulations. This is based on the exchange interaction between static and flying qubits [46]. There are many proposals for exploiting this scheme for applications in quantum information processing [46–50].

We examine here a scheme to generate an n-qubit W state in a system whose Hamiltonian takes a particular form: pairwise exchange interaction between all the qubits. We show that time evolution with this Hamiltonian for a certain time followed by single-qubit rotations leads to a W state. We discuss the implementation of such a system in the context of a system of static and flying qubits where spin torque drives the evolution. The static qubits are assumed to be noninteracting; however, repeated interactions with flying qubits can lead to effective exchange interaction between all pairs of qubits.

II. STATE-PREPARATION SCHEME

Consider a system of n spin-1/2's, each coupled with the others via Heisenberg exchange interaction so that the Hamiltonian can be written as

$$\mathcal{H} = J \sum_{i<j} \boldsymbol{\sigma}_i \cdot \boldsymbol{\sigma}_j, \tag{2}$$

[*] amritesh.iitb@gmail.com
[†] ashwin@ee.iitb.ac.in

where $\boldsymbol{\sigma_i} = (\sigma_x, \sigma_y, \sigma_z)$ denote the respective Pauli operators. The basis states of each qubit denoted by $|0\rangle$ and $|1\rangle$ are eigenfunctions of σ_z with eigenvalues ± 1, respectively. The Hamiltonian is block diagonal in the partitions of the computational basis $\mathcal{B}^n$ where all states with a fixed number of zeros and ones are considered in one partition. Restricted to an ordered partition of one-hot-encoded states (i.e., states where only one spin is in state 1), denoted by $\mathcal{B}_1^n = \{|u_i\rangle \in \mathcal{B}^n : |u_i\rangle = |0_1 \cdots 1_{n+1-i} \cdots 0_n\rangle\}$, the Hamiltonian can be written as

$$\mathcal{H} = J\left(\frac{(n-1)(n-4)}{2}\mathcal{I}_n + \begin{bmatrix} 0 & 2 & 2 & \dots \\ 2 & 0 & 2 & \dots \\ \vdots & \vdots & \ddots & \vdots \\ 2 & 2 & \dots & 0 \end{bmatrix}\right), \quad (3)$$

where $\mathcal{I}_n$ denotes the $n \times n$ identity matrix.

Starting from an unentangled state, $|\psi(0)\rangle = |u_i\rangle$, an evolved state at time t can be written as $|\psi(t)\rangle = \exp(-i\mathcal{H}t)\,|\psi(0)\rangle = a\,|u_i\rangle + b\sum_{j\neq i}|u_j\rangle$, with

$$a = \exp(iJnt) - i\frac{2}{n}\sin(Jnt), \quad b = -i\frac{2}{n}\sin(Jnt), \quad (4)$$

ignoring global phases (see Appendix A for the derivation). The coupling is turned off at $t = t_w$ when $|b|^2 = |a|^2 = 1/n$. The state thus formed, which we denote by $\overline{W}_n$, is close to the desired W_n state with exception of only a relative phase factor given by $\exp(i\theta) = a/b$ between $|u_i\rangle$ and others states in superposition. A z-axis rotation $R_z(\phi)$ of the excited qubit in the initial state yields the desired W_n state: $a\exp(i\phi)\,|u_i\rangle + b\sum_{j\neq i}|u_j\rangle$ up to a global phase if $\phi = 2m\pi - \theta$ for any integer m. This idea of sharing a single excited qubit among the others was previously shown in experiment for a system of three similarly interacting qubits [21]. We run into a problem extending this approach to a larger number of qubits. This can be immediately noted by observing that $|b|^2 = 1/n$ corresponds to the condition $\sin^2(Jnt_w) = n/4$, which cannot be satisfied for $n > 4$ for real t.

On the contrary, if we start from a product state of an entangled state W_q and $n-q$ qubits all in state $|0\rangle$, say,

$$|\psi(0)\rangle = |W_q\rangle \otimes |0\rangle^{\otimes n-q} = \frac{1}{\sqrt{q}}\sum_{i=1}^{q}|u_{n-i+1}\rangle\,, \quad (5)$$

then the evolved state at time t can be written as $|\psi(t)\rangle = c\sum_{i=1}^{q}|u_{n-i+1}\rangle + d\sum_{i=q+1}^{n}|u_{n-i+1}\rangle$, with $c = \frac{a+(q-1)b}{\sqrt{q}}$ and $d = \frac{bq}{\sqrt{q}} = \sqrt{q}b$. It would correspond to a $\overline{W}_n$ state if $|d|^2 = 1/n$. This translates to $\sin^2(Jnt) = \frac{n}{4q}$ and has a real solution t_w iff $n \leqslant 4q$. After reaching this state, the coupling is turned off, like before at time t_w, followed by correction of phase factors $\exp(i\theta) = c/d$ by single-qubit operations $R_z(\phi)$ of either the first q qubits or last $n-q$ qubits to reach the desired W_n state. The evolution time and z-axis rotation angle can be obtained from the expressions of a and b.

This paves a deterministic way to generate an arbitrary W_n state in $O(\log n)$ stages. In one possible path, every stage takes a jump of 4 times, starting from sharing a single excited state in stage 1 to reach a W_{4^1} state, from which a W_{4^2} state can be generated in stage 2 and so on to W_{4^k} in the kth stage assuming a sufficient number of $|0\rangle$ polarized qubits are available in each stage. A maximum of the $W_{4^{\lceil \log_4 n\rceil}}$ state can be generated in the $\lceil \log_4 n\rceil$th stage, which is sufficient for the required scheme since $n \leqslant 4^{\lceil \log_4 n\rceil}$, where $\lceil x\rceil$ indicates the smallest integer $\geqslant x$. Also, overhead cost of single-qubit gates at the kth stage for phase correction is 4^k, which entails that the total number of single-qubit gates required would be $O(4^{\lceil \log_4 n\rceil}) \approx O(n)$. Note, however, that these single-qubit gates are operated in parallel in each stage. A schematic for the algorithm is shown in Fig. 1.

The feasibility of expansion of W_q by a factor of 4 can be assessed by noting that the energy of the system, i.e., $\langle H\rangle$, remains conserved during the evolution. Neglecting the diagonal contributions to the Hamiltonian in Eq. (3), the energy of the initial state in Eq. (5) is $2J(q-1)$. An evolved state, if it corresponds to $\overline{W}_n$, can be written as $\frac{1}{\sqrt{n}}[\exp(i\theta)\sum_{i=1}^{q}|u_{n-i+1}\rangle + \sum_{i=q+1}^{n}|u_{n-i+1}\rangle]$, with energy $\frac{2J}{n}[2q(n-q)\cos\theta + q(q-1) + (n-q)(n-q-1)]$. Equating the energies before and after evolution gives $n = 4q\sin^2(\theta/2)$. Clearly, n can be, at most, $4q$, which is in agreement with the previous arguments. This also provides an expression for the phase correction required to obtain the W_n state.

Note that the all-coupled Hamiltonian can be written as $\mathcal{H} = (J/2)[\boldsymbol{\sigma}^2 - \sum_i \boldsymbol{\sigma}_i^2]$, which commutes with total spin angular momentum $\boldsymbol{\sigma} = \sum_i \boldsymbol{\sigma_i}$, i.e., $[\mathcal{H}, \boldsymbol{\sigma}] = 0$. This also entails that $\langle\boldsymbol{\sigma}^2\rangle$ should be conserved during the time evolution. Thus, energy conservation that restricts the expansion of equally distributed singly excited superpositions can be attributed to the fact that the system is not able to conserve total angular momentum for an expansion beyond a factor of 4, as argued previously. On the other hand, the phase-correction step discussed above requires single-qubit rotations on the first q qubits (or last $n-q$ qubits) to reach the W_n state. One way this can be done is by locally applying magnetic induction B along the z direction to the first q qubits for a certain time, i.e., time evolving the system under the Hamiltonian given by $H = -\gamma(B/2)\sum_{i=1}^{q}\sigma_{z,i}$, where γ is the gyromagnetic ratio. $\langle\boldsymbol{\sigma}^2\rangle$ changes during this evolution as it does not commute with this Hamiltonian. In the following we study a system that can emulate both Hamiltonians described above for desired operations under a suitable design.

III. SPIN-TORQUE SETTING

Consider a system of impurity spins embedded in a spin-coherent channel, equally spaced and placed sufficiently far apart that there is no direct interaction between them, as shown in the Fig. 2. There is hard barrier with perfect reflection on the left end, next to the first qubit. A barrier with a tunable transmission coefficient is present between the last qubit and a spin reservoir on the right end. In addition, barriers with tunable transmission (either 0 or 1) are present between the two qubits and between each qubit and a spin reservoir on top of the qubit. The spin reservoirs are held at certain spin potentials and are used to inject spin-polarized electrons into the channel. These itinerant spin carriers (flying qubits) collide with the immobile impurities (static qubits), get entangled with them, and finally return back after multiple

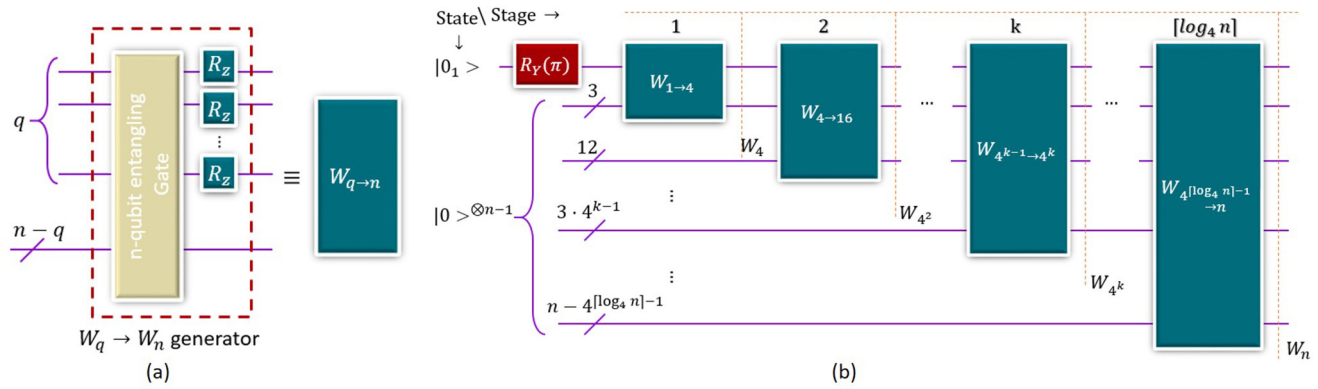

FIG. 1. W_n-state generation protocol. (a) W_q to W_n generator block: n-qubit entangling operation followed by phase-correction operations (single-qubit gates) on q qubits to generate a W_n state from a W_q state. (b) Circuit to generate the W_n state: Several W_q to W_n generator blocks are arranged successively in $\lceil \log_4 n \rceil$ to prepare a W_n state starting from $|0\rangle^{\otimes n}$ with one initial bit-flip gate required to excite a single qubit.

reflections, thereby affecting a spin-dependent rotation of the system's state. This can be seen as a spin-transfer-torque-like behavior in quantum scale systems.

Specific forms of this system were studied in [48] for single- and two-qubit gates and were also discussed in [49,50] for various applications. Ours is an adaptation with a greater number of qubits between the two barrier gates. While the states evolve, the role of time is taken up by the number of flying qubits injected (and eventually extracted) by the reservoir. We first consider the case where the barriers between the qubits are perfectly transmitting and the barriers between the qubit and the reservoir on the top are completely reflecting. Thus, we essentially have a system of n equally spaced qubits with a hard barrier to the left of the first qubit and a spin reservoir connected to the last qubit via a partially transmitting barrier (colored burnt umber in Fig. 2). Let's denote the density matrix of the static-qubit system after interaction

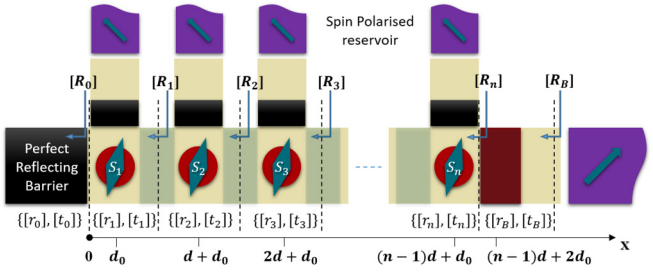

FIG. 2. Schematic of the system. n static qubits (colored red) in a spin-coherent channel (shaded yellow). There are barrier gates (colored black) to facilitate creation of standing waves and a reservoir (colored purple) to inject and extract spin-polarized carriers. Additional barrier gates (shaded light green) between the qubits are used to isolate the qubits when not in use. The distance between two successive qubits is d, while that between a qubit and a barrier gate is d_0. Individual qubits act as spin-dependent scatterers with reflection and transmission denoted by $[r]$ and $[t]$ matrices. Reflection matrices looking into the cascade of scatterers are also shown. In addition, each qubit is separately connected to spin reservoirs through transverse channels to enable single-qubit operations.

with m electrons by $\rho_s[m]$. When the $(m+1)$th electron is incident, we can write the initial state in the combined Hilbert space $H_f \otimes H_1 \otimes H_2 \otimes \cdots H_n$ as $\rho_f \otimes \rho_s[m]$, where ρ_f denotes the density matrix of the flying qubit. The unitary matrix describing the overall reflection process $\mathcal{R}_\mathcal{B}$ evolves it into $\mathcal{R}_\mathcal{B}(\rho_f \otimes \rho_s[m])\mathcal{R}_\mathcal{B}^\dagger$. The $(m+1)$th state of the n-qubit system can thus be obtained by taking a partial trace over the flying qubit's subspace:

$$\rho_s[m+1] = \mathrm{Tr}_f\left\{\mathcal{R}_B(\rho_f \otimes \rho_s[m])\mathcal{R}_B^\dagger\right\}. \tag{6}$$

The procedure to obtain $\mathcal{R}_B$ is deferred to Appendix. B. One can obtain Kraus operators $\{M_K\}$ relevant for this evolution. For $|0\rangle$ polarized electrons, the (i,j)th element of the matrix representation in the computational basis is given by $M_K^{i,j} = \langle K, i|\, \mathcal{R}_B\, |0, j\rangle$, where $|i\rangle, |j\rangle \in \mathcal{B}^n$ and K can be 0 or 1. (See Appendix. C for more discussion on Kraus operators.) With a proper design of system parameters M_0 alone can approximately evolve the system state, and its one-hot partition emulates a unitary evolution corresponding to the Hamiltonian given in Eq. (3), providing a use case for implementing the algorithm discussed in the previous section. The system parameters can be reduced to kd, kd_0, Γ, and Ω (since d_j always appears together with k in the expression for $\mathcal{R}_B$, we club them), where k is the wave vector of the injected electrons, d and d_0 are the spacing between static qubits and the distance of the barriers from static qubits, respectively, and Ω and Γ indicate the interaction strength of flying qubits with the static qubits and barriers. A scheme to probe appropriate regions in parameter space is also outlined in Appendix. C. For the purpose of illustrating the expansion scheme, we choose $(kd, kd_0) = (\pi, \pi/2)$ and $(\Gamma, \Omega) = (1000, 0.0001)$. One can attribute an effective interaction J_{eff} between these noninteracting static spins. Assume that one electron stays for a time δt in the channel and causes a small rotation in the Hilbert space. The evolution matrix is thus given by $U(\delta t) = \exp(-i\mathcal{H}\delta t) = 1 - i\mathcal{H}\delta t$. We indeed checked that the relation $M_0 \approx 1 - i\mathcal{H}\delta t$ can be satisfied (after correcting for phase factors) in the one-hot-encoded subspace to good accuracy. From this comparison we could also get the value of the effective exchange constant J_{eff} for unit δt, which is

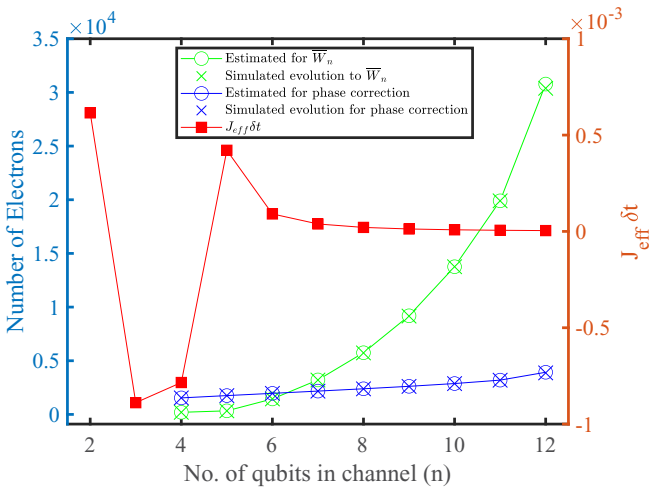

FIG. 3. Number of electrons required for evolution. Simulated number of electrons required for entangling evolution for the $\overline{W}_n$ state and for phase correction to get the W_n state starting from a W_3 state in the spin-torque setting for $3 < n \leqslant 12$. Corresponding estimations shown as data circles match well with the simulations. Also, variation of $J_{\text{eff}}\delta t$ as a function of the number of qubits shown on the right axis.

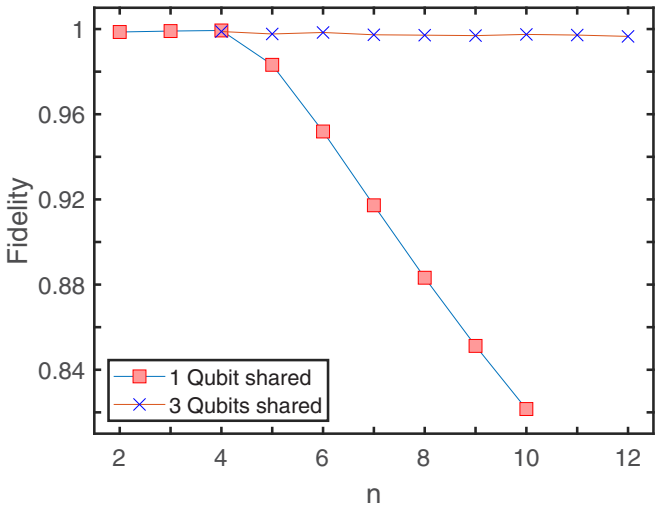

FIG. 4. Fidelity of obtained states. Fidelity of the n-qubit W state obtained using a single-qubit sharing procedure vs sharing a superposition of three singly excited qubits (a $W_{q=3}$ state) as a function of n.

plotted in Fig. 3 as a function of the number of qubits. One can see oscillation in J_{eff} followed by a decay as the number of qubits increases. This is reminiscent of the Ruderman-Kittel-Kasuya-Yosida oscillations in exchange coupling between two spins as a function of distance [51].

The above discussion shows that one can emulate the Hamiltonian given in Eq. (3) by the proper choice of parameters. Using this, once $\overline{W}_n$ is prepared, we raise the barrier between the last qubit and reservoir for no transmission, preventing further evolution. We also close the barriers between all the qubits. The next step required is single-qubit rotations of the appended qubits in the channel to perform the final phase correction. This is achieved by opening the barriers between appended qubits and the spin reservoirs on the top (see Fig. 2). Polarized electrons sequentially interacting with the qubit cause a rotation in the qubit's state. The state evolution is described by an equation [Eq. (B6)] similar to Eq. (6) with the number of static qubits equal to 1 and $\Gamma = 0$ (note that there is no partially transmitting barrier involved in this case). The interaction between flying qubits and the static qubit effectively gives rise to a rotation of the static qubit's spin along the polarization direction of the flying qubit. Once the rotation required for phase correction is achieved, the barrier is again set to perfect reflection, thereby stopping further evolution. The single-qubit operations are done simultaneously for all the qubits to be rotated. An example of how this method can be used to generate the W_3 state from the $|0\rangle$ state is described in Appendix C. Following the procedure for sharing a singly excited qubit excitation among others to generate a W_n state with a larger number of qubits in the channel, we observe that the fidelity obtained decreases considerably beyond ten qubits, as shown in Fig. 4. This is expected since it works only until $n = 4$, as proved in the previous section. We obtain much better fidelities in preparing the W_n state using another W_q state appended with $|0\rangle^{\otimes n-q}$ as the initial state. Figure 4 also shows fidelities associated with creation of a W_n state from the $W_{q=3}$ state. We see that fidelities remain $\geqslant$99.9% all the way up to $n = 4q = 12$ qubits. In this work we have used $F(\rho, |\psi\rangle) = \sqrt{\langle\psi|\,\rho\,|\psi\rangle}$ as the definition of fidelity for a general state described by ρ and a pure state $|\psi\rangle$ [1].

The stopping time t_w and hence the number of electrons N required to obtain the $\overline{W}_n$ state starting from W_q are given by $N = \frac{t_w}{\delta t} = \frac{1}{n|J_{\text{eff}}(n)|\delta t}\sin^{-1}\sqrt{\frac{n}{4q}}$. As shown in Fig. 3, the number of electrons obtained from this expression (green circle) and from complete numerical evolution (green cross) agree quite well. Also, comparing the Kraus operator M_0 for single-qubit rotation with the z-axis rotation operator $R_z(\delta\phi) = \exp(-i\sigma_z\delta\phi/2)$ gives the rotation caused by individual electrons $\delta\phi$. This is analogous to rotation under uniform magnetic field B_{eff} for a time δt. The stated comparison gives $\delta\phi = \gamma B_{\text{eff}}\delta t = 7.99 \times 10^{-4}$ rad, where γ is the gyromagnetic ratio of individual static qubits. The net rotation required for phase correction ϕ is determined from the phase factor $\exp(i\theta) = c/d$ of $\overline{W}_n$ and hence the number of electrons required for single-qubit rotations $\phi/\delta\phi$ can also be estimated. As shown in Fig. 3, this value (blue circle) agrees well with complete numerical evolution (blue cross). Note that the number of electrons required increases as q to n jumps grow steeper. The increase in the number of electrons is due to the decrease in J_{eff} for rotation of larger n. Thus, in this case nonmaximal jumps may be beneficial in terms of the number of electrons required. However, if a system can be designed where J_{eff} does not decrease as fast as J_{eff} obtained for this choice of parameters, we could reach W_n states quicker while taking maximum jumps. It should be noted that during the transition from the W_q state to the $\overline{W}_n$ state, the spin angular momentum of the static-qubit system is conserved. During the transition from the $\overline{W}_n$ state to the W_n state the single-qubit rotation operations change the spin angular momentum.

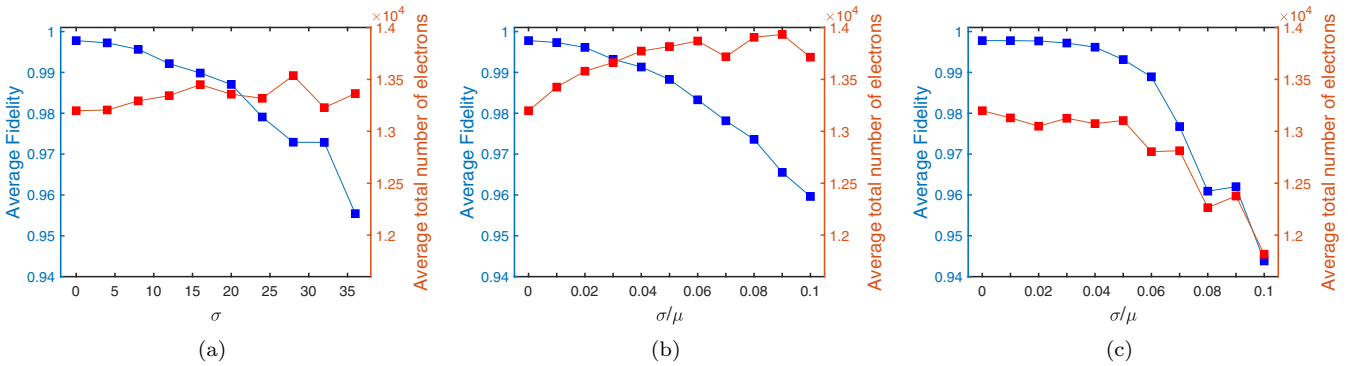

FIG. 5. Average fidelity obtained and the number of electrons required for preparation (entangling evolution plus phase-correction evolution) of the W_8 state from the W_2 state on introduction of nonidealities. Nonidealities are introduced assuming a normal distribution with mean μ and standard deviation σ. For each x data point, i.e., the (μ, σ) pair, 100 sample sets were simulated, followed by averaging corresponding data. Here, one sample set refers to the set of parameters sampled at each site. (a) Effect of nonideal transmission of barriers in between the qubits. Γ for the barriers is chosen from a distribution with $\mu = 0$. (b) Effect of uncertainty in the exchange interaction of flying and static qubits. The distribution from which Ω's were sampled had a mean of 0.0001. (c) Effect of nonideal distances between successive pairs of qubits. The parameters kd and kd_0 were respectively sampled from distributions with $\mu = \pi$ and $\pi/2$, and each set was adjusted uniformly to have a constant sum (explained in the main text).

IV. NONIDEALITIES IN DESIGN

There are a number of design considerations in this architecture similar to those discussed in [48]. We have assumed a 100% polarization for the reservoirs, which is seldom the case. However, it is not a primary requirement for the system to work, only that weaker polarization would incur more error in the evolution, as can be seen from Fig. 7 for three qubits, when undesired states outside the desired subspace states start sharing the superposition. Consider an example of preparing a W_8 state from a W_2 state. If we use reservoirs that are 30% polarized (achievable in silicon at low temperatures [52]), we can obtain a fidelity of 99.38% with about 28 000 electrons as opposed to a fidelity of 99.77% with about 13 000 electrons obtainable with reservoirs that are 100% polarized. Thus, it is possible to obtain states with good fidelities at the cost of more electrons. Another point is that the values of various parameters were optimized assuming 100% polarization. Optimization with 30% polarization can give us parameters which require fewer electrons.

The barrier gates (shaded light green in Fig. 2) are supposed to be completely transmitting while entangling the qubits (preparing the $\overline{W}_n$ state); that is, these gates can be described by spin-independent δ function barriers with $\Gamma = 0$ [see Eq. (B4)]. We modeled the nonideality in the gates by assuming that the Γ value of each gate is chosen randomly from a normal distribution with mean $\mu = 0$ and variance σ. For a given value of σ we chose 100 random samples and numerically obtained the fidelity in each case. The average fidelity as a function of σ is shown in Fig. 5(a). The average number of electrons required is also shown as it is an important parameter. It can be seen that even for $\sigma = 10$, we can get a fidelity of better than 99%. Comparing this to the $\Gamma = 10^3$ value of the partially transmitting gate, $\sigma = 10$ would correspond to 1% variation. To assess the effect of variability in Heisenberg coupling Ω of flying qubits with the individual static qubits, we assumed that different Ω are sampled from a normal distribution with mean $\mu = 10^{-4}$ and variance σ. The average fidelity and number of electrons required for 100 samples are shown in Fig. 5(b). It can be seen from Fig. 5(b) that we can achieve a fidelity of $> 99\%$ with $\sigma/\mu = 3\%$. In addition, the scheme requires us to shut off the channel from the reservoir. It typically takes about 10^4 electrons to prepare a W state. Experimentally, control over precise stopping can be challenging. For the above example we checked that we can easily tolerate ± 100 injected electrons from the exact amount required in both evolution and phase-correction steps with a negligible loss in fidelity. This corresponds to about 1% variation in the number of electrons. Passage of 10^4 electrons corresponds to passing a current of 160 nA for 10 ns [48]. A 1% variation then corresponds to ± 100 ps in the pulse width.

Variabilities in physical design can also affect the performance of our algorithm in this architecture. For example, the separation between the qubits may not be uniform when the design is realized. We can similarly assess its impact in reference to the example above of W_8 state preparation. We chose values of parameters kd and kd_0 from a normal distribution with mean $\mu = \pi$ for kd and mean $\mu = \pi/2$ for kd_0. The variance σ was chosen such that σ/μ is the same for both kd and kd_0. We imposed an additional constraint in the simulations that the sum of all local kd and kd_0 values in the channel equals the corresponding sum in the ideal case. Figure 5(c) shows the variation of average fidelity and number of electrons as a function of σ/μ. For average fidelity $> 99\%$, a variability of 5% can be tolerated. The imposition of the constraint here can be interpreted as fixing the channel length (the distance between the perfectly reflecting barrier and the partial barrier shaded burnt umber in Fig. 2) for a given value of k. It turns out that the above sum plays an important role in the state preparation in this architecture. In practice, one can satisfy this constraint by choosing a suitable value of k so that the k and channel-length product matches the ideal sum. This constraint seems to be relevant only for the entangling evolution part of the scheme. Indeed, that is true, and this part of the state preparation is majorly responsible for the drop in fidelity if only errors due to variability are considered. (The

numbers reported above are inclusive of the variability due to kd_0 in the phase-correction step.) If we do not impose the above constraint in the simulation, to get a fidelity of better than 99%, variation of 0.01% in σ/μ can be tolerated.

Note that we have considered monochromatic particles (electrons with single k values) to entangle static qubits. The value of J_{eff} and its sign is sensitive to the choice of k. The evolution can become inefficient due to the thermal average over wave vectors. One way to address this is to operate the system at low temperatures where only wave vectors near the Fermi surface are relevant. Another way in which high selectivity of k may be achieved is through use of additional resonant-tunneling barriers next to reservoirs. This will allow only electrons with wave vectors close to the desired k value to enter or exit the channel.

The flying qubit should not lose coherence during the multiple reflections during the W state preparation. This places a limit on the length of the channel and hence on the number of static qubits. However, large spin-coherence lengths have been obtained experimentally; for example, a spin-coherence length of 10 μm in Si at 85 K was reported in [53]. Use of low temperatures would enable a further increase in the number of static qubits in the channel.

V. TOWARDS COMPACT ARCHITECTURE

Geometrically, there are two essential requirements for the architecture for this proposal. First, a random qubit must be uniquely accessible to perform single-qubit manipulation. Second, it must allow n random qubits to be arranged in a one-dimensional fashion so that electrons from reservoirs can interact only successively for the multiqubit entanglement we have described above.

From Eq. (B5) in Appendix B it can be seen that the evolution dynamics is unaffected if the choice of d and d_0 is periodic with π/k. This enables us to stretch the one-dimensional arrangement of static qubits, as shown in Fig. 2, and create a more optimal arrangement of static qubits. Consider a meshed network of vertical and horizontal spin-coherent semiconductor channels where a planar lattice of the static qubits is embedded in the columns of the network, as shown in Fig. 6. Here, we can uniquely access individual qubits through each column. To get n qubits in a line, we just need to "needle" out a way through the channels as if the lattice were a two-dimensional "fabric." This would thus enable multiqubit entanglement. An example is shown in Fig. 6. Three target qubits to be entangled are shown as red spheres. The path that would be opened for electrons to flow is shown in transparent green. To perform an entangling evolution, electrons are injected from the reservoir connected to a vertical column containing the partial barrier shown in pink. Single-qubit operations would be performed similarly, but the transport would be restricted to only individual columns (columns would be isolated; barriers can be raised so that no electrons are allowed to leak horizontally from the column containing the target qubit).

Each intersection i of horizontal and vertical channels is provided with six barrier gates $G_{i,\hat{k}}$, where $\hat{k} = \pm x, \pm y, \pm z$ is the orientation of the face of the gate facing outward from the node. The potential of each gate is assumed to be fully

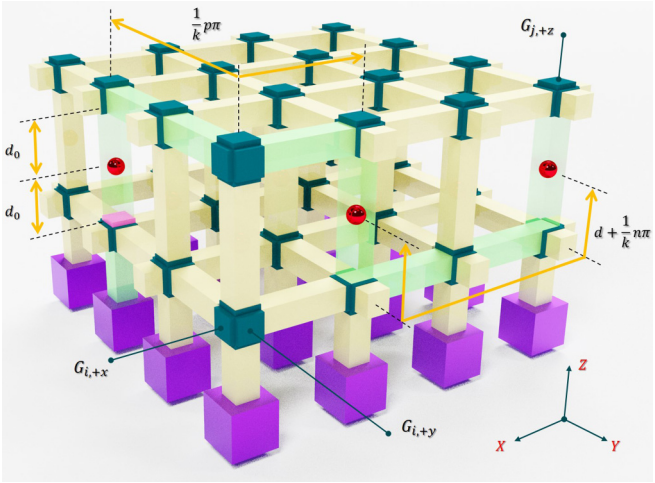

FIG. 6. Schematic of the proposed architecture. Static qubits (red) embedded in the columns of a spin-coherent channel (bright yellow) grid. Hard barriers $G_{i,\hat{k}}$ (dark turquoise) guide the electrons along a path (transparent and green) shown for three-qubit entanglement. The partial barrier which is also a part for implementing the scheme is colored pink. The distance between a qubit and the gates facing it in each column is d_0, while the distance of the farther gates is roughly $d/2$. The Manhattan distance between any two nodes on a horizontal level is an integer multiple of π/k. This ensures any two qubits are separated effectively by a distance d up to certain tolerances governed by optimization of parameters.

controllable such that the gate can serve as a hard barrier or a partial one or be completely open to the flow of electrons. Hard barriers can be used for isolation of qubits when not operated and can redirect the flow of flying carriers between the horizontal and vertical channels and can be used for perfect refection (R_0 in Fig. 2) necessary to implement the proposed scheme. The gates are required to be open while the flow of electrons is guided through an intersectional node. Flying electrons can be supplied from desired spin-polarized reservoirs connected to the vertical columns. The model we have used is a one-dimensional model, where right-angle bends in the path of the electron do not matter. In a realistic design, we need to consider at least a two-dimensional model, where right-angle bends would affect the propagation of electrons. Such design optimization is beyond the scope of the present paper.

Note that this entire procedure can also be used to generate a pure superposition of all one-cold entangled states if we use down-spin reservoirs in which the evolution would happen in a one-cold-encoded subspace. This can be equivalently seen by interchanging the roles of zeros and ones. The architecture may also be utilized for preparation of generalized Dicke states and will be taken up in a future work.

VI. CONCLUSION

In summary we have presented a scheme to generate the W_n state in systems with all-to-all exchange coupling between the constituent spins. We have shown that a single-qubit sharing scheme works only up to four qubits and have suggested an improvement to start from another W state of smaller

cardinality, thereby outlining a procedure to generate a W_n state in $O(\log n)$ stages. In the improved procedure only the one-hot-encoded subspace is utilized, so physical systems which are equivalent in just this subspace also can be utilized in this scheme. We have shown that spin-torque quantum computing architecture based on static- and flying-qubit interactions is one such avenue where it can be engineered; that is, the evolution operator can be made to emulate the evolution by an all-to-all coupling Hamiltonian in a reduced subspace.

ACKNOWLEDGMENTS

We acknowledge the support of the Department of Science and Technology (DST), government of India, through Project No. SR/NM/NS-1112/2016 and the Science and Engineering Research Board (SERB) through Project No. EMR/2016/007131. We also thank Prof. S. Vinjanampathy for his valuable comments.

APPENDIX A: DERIVATION OF COEFFICIENTS a and b

In Sec. II of the main text, we give an expression for the evolved state in terms of coefficients a and b [Eq. (4)]. Let's look at it in detail here.

To simplify the calculations, we write the Hamiltonian as $H = 2J\mathbb{1}_n$, where $\mathbb{1}_n$ denotes an $n \times n$ all-ones matrix. We can do this by adjusting the diagonal terms which contribute no more than global phases to evolved states. We can note that the W_n state is an eigenfunction of H with eigenvalue $2Jn$ and all other $n-1$ eigenvalues are zero. Let us denote these states by $|\psi_1\rangle, |\psi_2\rangle, \ldots, |\psi_{n-1}\rangle$ and state W_n by $|\psi_n\rangle$. We start with initial state at $t = 0$, $|\phi(0)\rangle = |u_i\rangle = |00\cdots1_i\cdots0\rangle$, which can be written in the above basis of eigenfunctions of H as $\sum_j c_j |\psi_j\rangle$, with $c_j = \langle\psi_j|u_i\rangle$. The evolved state can thus be written as

$$\begin{aligned}|\phi(t)\rangle &= \sum_j c_j \exp(-iE_j t)\,|\psi_j\rangle \\ &= \exp(-iE_n t)c_n\,|\psi_n\rangle + \sum_{j\neq n} c_j\,|\psi_j\rangle \\ &= \frac{1}{\sqrt{n}}[\exp(-iE_n t) - 1]\,|\psi_n\rangle + |u_i\rangle\,,\end{aligned}$$

where we have utilized the fact that $c_n = \langle\psi_n|u_i\rangle = \frac{1}{\sqrt{n}}$.

Our aim is to find the coefficients of vectors of the computational basis describing $|\phi(t)\rangle$. With the form obtained above we can easily obtain the coefficients as $\langle u_j|\phi(t)\rangle = \frac{1}{\sqrt{n}}[\exp(-iE_n t) - 1]\,\langle u_j|\psi_n\rangle + \langle u_j|u_i\rangle$, which can be simplified as $\frac{1}{n}[\exp(-i2Jnt) - 1] + \delta_{ij}$. Note $b = \langle u_{j\neq i}|\psi(t)\rangle$. Thus,

$$\begin{aligned}b &= \frac{1}{n}\exp(-iJnt)[\exp(-iJnt) - \exp(iJnt)] \\ &= -\frac{2i}{n}\exp(-iJnt)\sin(Jnt),\end{aligned}$$

and similarly,

$$\begin{aligned}a &= \langle u_i|\psi(t)\rangle \\ &= \exp(-iJnt)\left[\exp(iJnt) - \frac{2i}{n}\sin(Jnt)\right].\end{aligned}$$

Neglecting the common phase factor of $\exp(-iJnt)$, the expressions obtained for a and b match the expressions given in Eq. (4) in the main text.

APPENDIX B: OBTAINING REFLECTION MATRIX R_B

In reference to Fig. 2 in the main text, the interaction between the flying and jth static qubit at location x_j is governed by the exchange Hamiltonian

$$\mathcal{H} = J_0\boldsymbol{\sigma_f}\cdot\boldsymbol{\sigma_j}\delta(x - x_j), \tag{B1}$$

where $\boldsymbol{\sigma_f}$ and $\boldsymbol{\sigma_j}$ denote corresponding Pauli operators and J_0 is the exchange strength. The transmission and reflection corresponding to this spin-dependent δ scatterer can be written as t_j and $r_j = t_j - \mathcal{I}$, with

$$t_j = [\mathcal{I} + i\Omega\boldsymbol{\sigma_f}\cdot\boldsymbol{\sigma_j}]^{-1}, \tag{B2}$$

where $\Omega = J_0/\hbar v$, v is the velocity of injected electrons in the channel, and $\mathcal{I}$ is an identity matrix of dimension $2^{n+1}\times 2^{n+1}$. A cascade of the jth scatterer from the $(j-1)$th scatterer modifies its reflection as

$$R_j = r_j + e^{2ikd_j}t_j(\mathcal{I} - e^{2ikd_j}R_{j-1}r_j)^{-1}R_{j-1}t_j, \tag{B3}$$

where k is the wave vector of the injected electrons and d_j is the distance of the jth scatterer from the $(j-1)$th scatterer.

These interactions are quite weak but can be enhanced with proper placement of static impurities and barrier gates which facilitate formation of standing waves and thereby stronger interaction. These barrier gates have spin-independent transmission

$$t_B = \frac{1}{(1+i\Gamma)}\mathcal{I} \tag{B4}$$

and reflection given by $r_B = t_B - \mathcal{I}$. The hard barrier (R_0) on the leftmost side is characterized by $r_B = -\mathcal{I}$. The overall reflection matrix $\mathcal{R}_\mathcal{B}$ for the cascade of n such scatterers and barrier gates (see Fig. 2) can be obtained using Eq. (B3) as

$$\mathcal{R}_\mathcal{B} = r_B + e^{2ikd_0}t_B(\mathcal{I} - e^{2ikd_0}R_n r_B)^{-1}\hat{r}_n t_B. \tag{B5}$$

On the other hand, for single-qubit rotations, the reflection matrix can be obtained by substituting $j = 1$ in Eq. (B3), where d_1, being the distance of the qubit "scatterer" from the "perfectly reflecting scatterer" (hard barrier), is d_0. Rewriting the matrix for single-qubit rotations for clarity. Since there are no partially reflecting barriers involved, $\Gamma = 0$ implies $t_B = \mathcal{I}$ and hence there is no modification to R_1 as far as single-qubit rotations are concerned according to Eq. (B5). Therefore we write R_1 for single qubit rotations for clarity as

$$\mathcal{R}_{B|\text{single qubit}} = r + e^{2ikd_0}t(\mathcal{I} - e^{2ikd_j}R_0 r)^{-1}R_0 t. \tag{B6}$$

Here, we have omitted the subscripts for the r and t matrices which correspond to the target qubit in rotation. Like before, R_0 is taken to be $-\mathcal{I}$ which corresponds to a perfectly reflecting barrier.

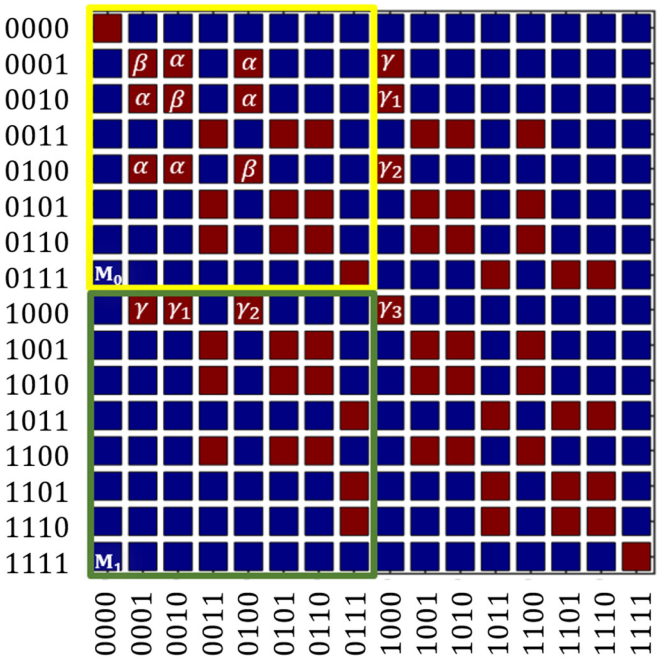

FIG. 7. $\mathcal{R}_B$ for three qubits in the channel. Nonzero elements of the overall reflection matrix $\mathcal{R}_B$ are colored red, while the zero elements are colored blue independent of the parameters. The Kraus operators M_0 and M_1 are partitions of the full $\mathcal{R}_B$, highlighted in yellow and green. The terms relevant to the evolution are α and β as labeled, while γ, γ_1, and γ_2 give undesired superpositions in evolution.

APPENDIX C: CHOICE OF SYSTEM PARAMETERS AND DESIGN TRADE-OFF

To illustrate the scheme we have used reservoirs that inject only $|0\rangle$ polarized electrons, in which case the relevant Kraus operators for this evolution in the subspace of n qubits, $M_K^{i,j} = \langle K, i|\,\mathcal{R}_B\,|0, j\rangle$, are essentially the following partitions of the overall reflection matrix $\mathcal{R}_B$ if described in computational basis $\mathcal{B}^{n+1}$:

$$M_0 = \mathcal{R}_{\mathcal{B}}(1 : 2^n, 1 : 2^n), \tag{C1a}$$

$$M_1 = \mathcal{R}_{\mathcal{B}}(2^n + 1 : 2^{n+1}, 1 : 2^n), \tag{C1b}$$

satisfying $M_0^\dagger M_0 + M_1^\dagger M_1 = \mathcal{I}_{2^n}$. The first set of indices indicates the rows, while the second corresponds to the columns of the matrix description. The evolution of Eq. (6) can be rephrased as

$$\rho_s[m+1] = M_0\rho_s[m]M_0^\dagger + M_1\rho_s[m]M_1^\dagger. \tag{C2}$$

The elements of matrices M_0 and M_1 depend on the values of four parameters, kd, kd_0, Γ, and Ω (since d_j always appears together with k, we club them). We need to choose these values such that the evolution of static qubits given by Eq. (C2) can be approximated by unitary evolution corresponding to the Hamiltonian in Eq. (3). For this, we analyze the system with three static qubits in the channel. The optimized values of the parameters obtained are then used for all cases. Irrespective of the specific values of the aforementioned parameters, the operator $\mathcal{R}_B$ takes the form shown in Fig. 7. We can identify the aforementioned Kraus operators in the overall reflection matrix. Considering the one-hot-encoded subspace of M_0 operator, we see that it can emulate the desired unitary, provided $|\beta|^2 + 2|\alpha|^2 = 1$. The blocks of a block-diagonal unitary operator are also unitary. Thus, if we look for a parameter space where $M_0^\dagger M_0 \approx \mathcal{I}_{2^n}$ or $M_1^\dagger M_1 \approx O_{2^n}$, the system would be evolved nearly unitarily by M_0 according to Eq. (C2).

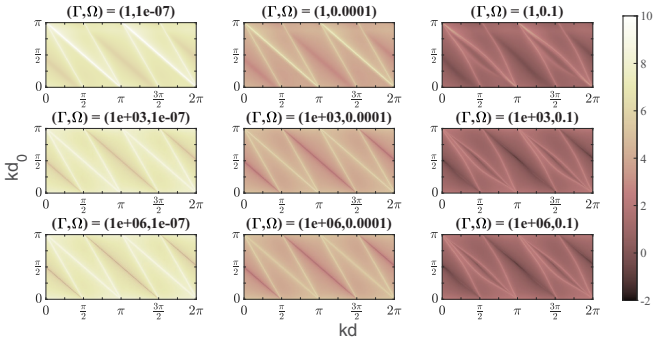

FIG. 8. P_3 as a function of kd and kd_0 for different values of (Γ, Ω) about $(1000, 0.0001)$. Good choices of kd and kd_0 occur around a negative sloped line about $(\pi, \pi/2)$.

It is important to note that the off-diagonal term, α, of M_0 in its one-hot-encoded subspace is responsible for distributing the amplitude of an excited qubit among other qubits. So we should also try to maximize $|\alpha|$ when looking for the optimal space in addition to trying to make $M_1^\dagger M_1 \approx O_{2^n}$. We define a figure of merit (P), which we seek to minimize over all the parameters, as follows:

$$\mathrm{P}_n = \log_{10}\left(\frac{\|\mathrm{M}_1\|_F}{|\alpha|}\right), \tag{C3}$$

$\|M_1\|_F$ is the Frobenius norm of M_1 and n is the number of qubits in the channel.

Figure 8 shows the variation of P_3 as a function of kd and kd_0. A global minimum in this space occurs at $(kd, kd_0) = (\pi, \pi/2)$. P_3 does not change much as long as we remain in the negative-slope region about the stated coordinate. Also, it gets affected only when we change (Γ, Ω) by orders of magnitude. So it is quite robust against the choice of interaction strength parameters. Similarly, Fig. 9 shows the variation of

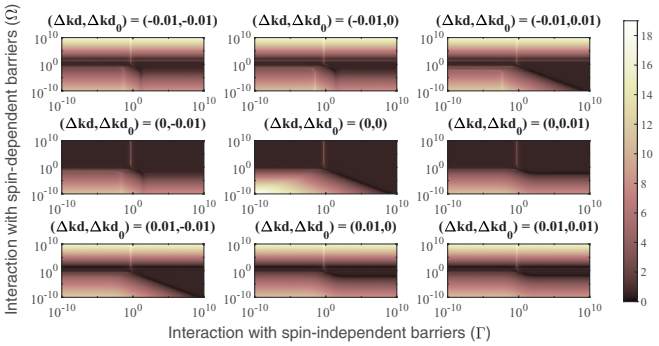

FIG. 9. P_3 as a function of Γ and Ω for different choices of (kd, kd_0) about $(\pi, \pi/2)$. Δkd and Δkd_0 represent the offsets $kd - \pi$ and $kd_0 - \pi/2$.

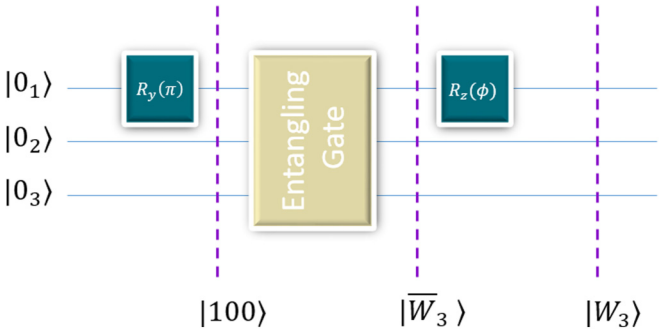

FIG. 10. Quantum circuit for generation of the W_3 state.

P_3 with Γ and Ω corresponding to tolerances in the choices of (kd, kd_0) about $(\pi, \pi/2)$. There is no common region of choices of Γ and Ω among different plots, implying P_3 is very sensitive to the choice of (kd, kd_0). This indicates that given a geometry, i.e., a choice of (d, d_0), only electrons with a certain wave vector can cause desired rotations which will be provided by the spin reservoirs connected to the channel. Our system implements single-qubit rotations in the way discussed in [48] for phase correction, as discussed previously, which requires either Ω or kd_0 to be small. This is contrary to the observation from Fig. 8, where a general decreasing trend for P_3 is observed with increasing Ω. This implies a design trade-off in the choice of parameters. Also, these parameters can affect the overall speed of the system in terms of the total number of electrons required, and further optimization can be done. We choose $(kd, kd_0) = (\pi, \pi/2)$ and $(\Gamma, \Omega) = (1000, 0.0001)$, which are good enough parameters for the purpose of demonstration.

As an example, let's look at how one can prepare the W_3 state using the scheme discussed in the main text in the setting of spin-torque quantum computing architecture. Consider the quantum circuit shown in Fig. 10. Assume an initial state $|000\rangle$ for the three qubits in the channel. Performing a rotation with the y-polarized reservoir connected only to the first qubit as prescribed in [48], we prepare a $|100\rangle$ state. After that we let open the $+z$-polarized reservoir injecting electrons in state $|0\rangle$, commonly connected to the spin-chain system that enables an entangling evolution of the system governed by Eq. (6). Variation of diagonal components of the system's density matrix expressed in $\mathcal{B}_1^3$ with the number of electrons while in this phase is shown in Fig. 11. We turn off the coupling to the reservoirs when the three curves intersect at a point to stop further evolution. The state of the system at this stage is actually $\overline{W}_3$. All diagonal components are nearly equal, and ideally, their product equals $1/27$. As far as simulations are concerned, we stop at the point when the product of diagonal entries reaches a maximum. Now, for the phase-correction step we perform a single-qubit manipulation of the first qubit like before but with z-polarized spins. This final evolution eventually leads to a W_3 state, after which we close the gates. To assess the quality of the W_3 state obtained, we use fidelity, which determines the closeness of two states. In the scheme described above we stop the phase-correction step when the fidelity between the evolving state and an ideal W_n state

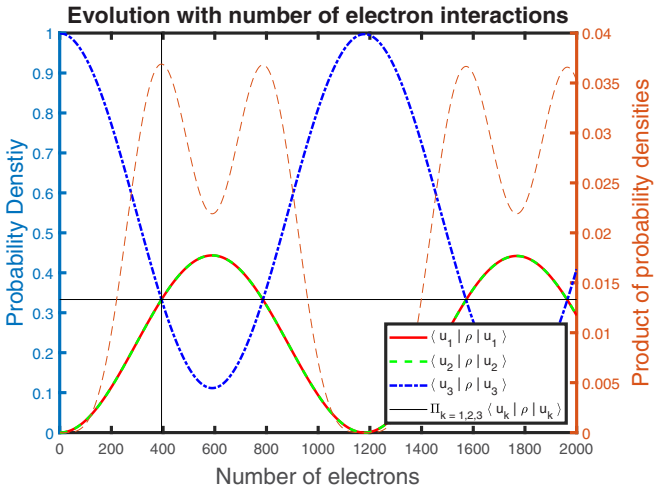

FIG. 11. Three-qubit evolution. Evolution of diagonal entries (left axis) and their product (right axis) of the system's density matrix represented in $\mathcal{B}_1^3$. The vertical line (black) marks the point when the product reaches the maximum, supposedly $1/27$, in this case indicating the creation of the $\overline{W}_3$ state. The horizontal line (black) has an ordinate equal to $1/3$ and indicates that the evolved desired density-matrix components intersect when close to ideal value $1/3$.

reaches a maximum. For the three-qubit case we obtain a fidelity of ∼99.9%. The simulated density matrix components of the state obtained after the entangling evolution and phase correction steps are shown in Fig. 12

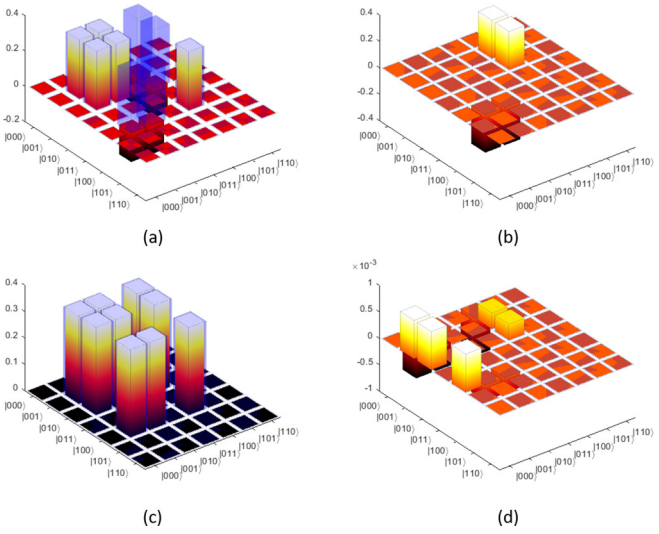

FIG. 12. Density-matrix components. (a) and (c) Real and (b) and (d) imaginary parts of the obtained density matrix before and after phase correction, respectively. The blue translucent and slightly thicker bars correspond to the density matrix of the desired W_3 state. There is a good match between the obtained and expected density matrices. The blue bars sheath the bars of the real part of the obtained density matrix after phase correction with negligible error in the imaginary part, as also reflected by the obtained fidelity of 99.9%.

[1] M. A. Nielsen and I. L. Chuang, *Quantum Computation and Quantum Information* (Cambridge University Press, Cambridge, 2010).

[2] F. Arute, K. Arya, R. Babbush, D. Bacon, J. C. Bardin, R. Barends, R. Biswas, S. Boixo, F. G. Brandao, D. A. Buell *et al.*, Quantum supremacy using a programmable superconducting processor, Nature (London) **574**, 505 (2019).

[3] Y. He, S. Gorman, D. Keith, L. Kranz, J. Keizer, and M. Simmons, A two-qubit gate between phosphorus donor electrons in silicon, Nature (London) **571**, 371 (2019).

[4] W. Dür, G. Vidal, and J. I. Cirac, Three qubits can be entangled in two inequivalent ways, Phys. Rev. A **62**, 062314 (2000).

[5] G. Teklemariam, E. M. Fortunato, M. A. Pravia, Y. Sharf, T. F. Havel, D. G. Cory, A. Bhattaharyya, and J. Hou, Quantum erasers and probing classifications of entanglement via nuclear magnetic resonance, Phys. Rev. A **66**, 012309 (2002).

[6] A. Cabello, Bell's theorem with and without inequalities for the three-qubit Greenberger-Horne-Zeilinger and *W* states, Phys. Rev. A **65**, 032108 (2002).

[7] A. Cabello, Two qubits of a *W* state violate Bell's inequality beyond Cirel'son's bound, Phys. Rev. A **66**, 042114 (2002).

[8] B. Çakmak, S. Campbell, B. Vacchini, Ö. E. Müstecaplıoğlu, and M. Paternostro, Robust multipartite entanglement generation via a collision model, Phys. Rev. A **99**, 012319 (2019).

[9] A. Neven, J. Martin, and T. Bastin, Entanglement robustness against particle loss in multiqubit systems, Phys. Rev. A **98**, 062335 (2018).

[10] W. Liu, Y.-B. Wang, and Z.-T. Jiang, An efficient protocol for the quantum private comparison of equality with W state, Opt. Commun. **284**, 3160 (2011).

[11] C. Zhu, F. Xu, and C. Pei, W-state analyzer and multiparty measurement-device-independent quantum key distribution, Sci. Rep. **5**, 17449 (2015).

[12] V. Lipinska, G. Murta, and S. Wehner, Anonymous transmission in a noisy quantum network using the *W* state, Phys. Rev. A **98**, 052320 (2018).

[13] Z. Zhao, Y.-A. Chen, A.-N. Zhang, T. Yang, H. J. Briegel, and J.-W. Pan, Experimental demonstration of five-photon entanglement and open-destination teleportation, Nature (London) **430**, 54 (2004).

[14] J. Joo, Y.-J. Park, S. Oh, and J. Kim, Quantum teleportation via a W state, New J. Phys. **5**, 136 (2003).

[15] N. Sangouard, C. Simon, H. de Riedmatten, and N. Gisin, Quantum repeaters based on atomic ensembles and linear optics, Rev. Mod. Phys. **83**, 33 (2011).

[16] E. D'Hondt and P. Panangaden, The computational power of the W and GHZ states, Journ. Quantum Inf. and Comp. **6**, 173 (2005).

[17] J. Preskill, Quantum Computing in the NISQ era and beyond, Quantum **2**, 79 (2018).

[18] A. Galiautdinov, Simple protocol for generating W states in resonator-based quantum computing architectures, arXiv:1203.5534.

[19] Y.-H. Kang, Y.-H. Chen, Q.-C. Wu, B.-H. Huang, J. Song, and Y. Xia, Fast generation of W states of superconducting qubits with multiple Schrödinger dynamics, Sci. Rep. **6**, 36737 (2016).

[20] X.-F. Ye and M.-F. Chen, Generating W state with qubits of superconducting quantum interference devices via adiabatic passage, Commun. Theor. Phys. **55**, 868 (2011).

[21] M. Neeley, R. C. Bialczak, M. Lenander, E. Lucero, M. Mariantoni, A. O'connell, D. Sank, H. Wang, M. Weides, J. Wenner *et al.*, Generation of three-qubit entangled states using superconducting phase qubits, Nature (London) **467**, 570 (2010).

[22] N. Kiesel, M. Bourennane, C. Kurtsiefer, H. Weinfurter, D. Kaszlikowski, W. Laskowski, and M. Zukowski, Three-photon W-state, J. Mod. Opt. **50**, 1131 (2003).

[23] B.-S. Shi and A. Tomita, Schemes for generating W state of paths and w state of polarization photons, arXiv:quant-ph/0208170.

[24] X. B. Zou, K. Pahlke, and W. Mathis, Generation of an entangled four-photon *W* state, Phys. Rev. A **66**, 044302 (2002).

[25] Y. Li and T. Kobayashi, Four-photon *W* state using two-crystal geometry parametric down-conversion, Phys. Rev. A **70**, 014301 (2004).

[26] T. Tashima, Ş. K. Özdemir, T. Yamamoto, M. Koashi, and N. Imoto, Elementary optical gate for expanding an entanglement web, Phys. Rev. A **77**, 030302(R) (2008).

[27] J. Heo, C. Hong, S.-G. Choi, and J.-P. Hong, Scheme for generation of three-photon entangled W state assisted by cross-Kerr nonlinearity and quantum dot, Sci. Rep. **9**, 1 (2019).

[28] C. Yesilyurt, S. Bugu, F. Ozaydin, A. A. Altintas, M. Tame, L. Yang, and Ş. K. Özdemir, Deterministic local doubling of W states, J. Opt. Soc. Am. B **33**, 2313 (2016).

[29] H. Häffner, W. Hänsel, C. Roos, J. Benhelm, M. Chwalla, T. Körber, U. Rapol, M. Riebe, P. Schmidt, C. Becher *et al.*, Scalable multiparticle entanglement of trapped ions, Nature (London) **438**, 643 (2005).

[30] S. S. Sharma, E. de Almeida, and N. K. Sharma, Multipartite entanglement of three trapped ions in a cavity and W-state generation, J. Phys. B **41**, 165503 (2008).

[31] N. Yu and M. Ying, Optimal simulation of three-qubit gates, arXiv:1301.3727.

[32] F. Diker, Deterministic construction of arbitrary *W* states with quadratically increasing number of two-qubit gates, arXiv:1606.09290.

[33] Ş. K. Özdemir, E. Matsunaga, T. Tashima, T. Yamamoto, M. Koashi, and N. Imoto, An optical fusion gate for W-states, New J. Phys. **13**, 103003 (2011).

[34] S. Bugu, C. Yesilyurt, and F. Ozaydin, Enhancing the *W*-state quantum-network-fusion process with a single Fredkin gate, Phys. Rev. A **87**, 032331 (2013).

[35] Y. Sheng, J. Pan, R. Guo, L. Zhou, and L. Wang, Efficient n-particle W state concentration with different parity check gates, Sci. China Phys. Mech. Astron. **58**, 1 (2015).

[36] E. A. Martinez, T. Monz, D. Nigg, P. Schindler, and R. Blatt, Compiling quantum algorithms for architectures with multi-qubit gates, New J. Phys. **18**, 063029 (2016).

[37] S. Bandyopadhyay and M. Cahay, *Introduction to Spintronics* (CRC Press, Boca Raton, FL, 2015).

[38] J. C. Slonczewski, Current-driven excitation of magnetic multilayers, J. Magn. Magn. Mater. **159**, L1 (1996).

[39] L. Berger, Emission of spin waves by a magnetic multilayer traversed by a current, Phys. Rev. B **54**, 9353 (1996).

[40] S. Bhuktare, A. S. Shukla, H. Singh, A. Bose, and A. A. Tulapurkar, Direct observation of the reciprocity between spin current and phonon interconversion, Appl. Phys. Lett. **114**, 052402 (2019).

[41] A. Bose, S. Dutta, S. Bhuktare, H. Singh, and A. A. Tulapurkar, Sensitive measurement of spin-orbit torque driven ferromagnetic resonance detected by planar Hall geometry, Appl. Phys. Lett. **111**, 162405 (2017).

[42] A. Bose, D. D. Lam, S. Bhuktare, S. Dutta, H. Singh, Y. Jibiki, M. Goto, S. Miwa, and A. A. Tulapurkar, Observation of Anomalous Spin Torque Generated by a Ferromagnet, Phys. Rev. Appl. **9**, 064026 (2018).

[43] A. Bose, A. K. Shukla, K. Konishi, S. Jain, N. Asam, S. Bhuktare, H. Singh, D. D. Lam, Y. Fujii, S. Miwa *et al.*, Observation of thermally driven field-like spin torque in magnetic tunnel junctions, Appl. Phys. Lett. **109**, 032406 (2016).

[44] A. Bose and A. A. Tulapurkar, Recent advances in the spin Nernst effect, J. Magn. Magn. Mater. **491**, 165526 (2019).

[45] A. Bose, S. Bhuktare, H. Singh, S. Dutta, V. Achanta, and A. Tulapurkar, Direct detection of spin Nernst effect in platinum, Appl. Phys. Lett. **112**, 162401 (2018).

[46] G. Cordourier-Maruri, F. Ciccarello, Y. Omar, M. Zarcone, R. De Coss, and S. Bose, Implementing quantum gates through scattering between a static and a flying qubit, Phys. Rev. A **82**, 052313 (2010).

[47] A. De Pasquale, K. Yuasa, and H. Nakazato, State tomography of a qubit through scattering of a probe qubit, Phys. Rev. A **80**, 052111 (2009).

[48] B. Sutton and S. Datta, Manipulating quantum information with spin torque, Sci. Rep. **5**, 17912 (2015).

[49] A. Kulkarni, S. Prajapati, and B. K. Kaushik, Transmission coefficient matrix modeling of spin-torque-based n-qubit architecture, IEEE Trans. Very Large Scale Integr. (VLSI) Syst. **26**, 1461 (2018).

[50] A. Kulkarni and B. K. Kaushik, Spin-torque-based quantum fourier transform, IEEE Trans. Magn. **55**, 1 (2019).

[51] P. Bruno and C. Chappert, Ruderman-Kittel theory of oscillatory interlayer exchange coupling, Phys. Rev. B **46**, 261 (1992).

[52] B. T. Jonker, G. Kioseoglou, A. T. Hanbicki, C. H. Li, and P. E. Thompson, Electrical spin-injection into silicon from a ferromagnetic metal/tunnel barrier contact, Nat. Phys. **3**, 542 (2007).

[53] B. Huang, D. J. Monsma, and I. Appelbaum, Coherent spin Transport Through a 350 Micron Thick Silicon Wafer, Phys. Rev. Lett. **99**, 177209 (2007).